Available online at www.sciencedirect.com
ScienceDirect
Journal of Nuclear Materials 357 (2006) 97–104
journal of nuclear materials
www.elsevier.com/locate/jnucmat

Study on control of oxygen concentration in lead–bismuth flow using lead oxide particles

Masatoshi Kondo [a], Minoru Takahashi [b,*], Kuniaki Miura [c], Tatsuya Onizawa [c]

[a] Department of Nuclear Engineering, Graduate School of Science and Engineering, Tokyo Institute of Technology, N1-18, 2-12-1, O-okayama, Meguro-ku, Tokyo 152-8550, Japan
[b] Research Laboratory for Nuclear Reactors, Tokyo Institute of Technology, N1-18, 2-12-1, O-okayama, Meguro-ku, Tokyo 152-8550, Japan
[c] R&D Sect., Sukegawa Electric Co., Ltd., 3-19-5, Namekawahon-cho, Hitachi, Ibaraki 317-0051, Japan

Received 25 June 2005; accepted 31 May 2006

Abstract

Performance of mass exchanger type oxygen control system for the control of oxygen concentration in a flowing lead–bismuth (Pb–Bi) was investigated in a low temperature region of a Pb–Bi circulation loop. Oxygen dissolved and diffused from lead oxide (PbO) particles into the melt or oxide precipitated in the mass exchanger. The electromotive force (EMF) of an oxygen sensor installed in a high temperature region of the loop indicated the changes of oxygen concentration in the loop with the temperature changes of the PbO particles reasonably. The measured EMF agreed well with theoretical result obtained using $\Delta G^0_{\text{Pb–Bi–O equation}}$ in the Nernst equation. The expression of oxygen solubility in the melt in the mass exchanger, C_s, was derived from the data as $\log C_s = A + B/T$, where the constant A ranged from -4000 to -4600, and the constant B ranged from 1 to 3.5 depending on the temperature of the melt.

PACS: 81.30.Hh; 81.65.Mq; 82.30.Hk; 82.60.−s; 82.60.Hc

1. Introduction

Conceptual designs of lead–bismuth (45Pb–55Bi) cooled fast reactors (LFRs) and Pb–Bi target type accelerator driven system (ADS) have been proposed by a number of researchers [1–5]. The compatibility of cladding, structural and window materials in the Pb–Bi flow at high temperature is one of the critical issues.

A self-healed oxide layer formed on steel surface inhibits a liquid metal corrosion [6], and reduces the corrosion rate in the flowing Pb–Bi [7]. In order to keep a stable condition of the self-healed layer, an oxygen content in the Pb–Bi should be controlled adequately by an oxygen control system.

One of the control methods of oxygen concentration in liquid lead alloy is a chemical reaction of a mixture gas of H_2, steam and Ar with the melt. The controllability of this method was reported in Refs. [6,8]. The reaction rate increases at higher temperature, and the equilibrium of oxygen potentials in the gas and in the melt can be attained faster by increasing the gas-melt contact area. However,

* Corresponding author. Tel./fax: +81 3 5734 2957.
E-mail address: mtakahas@nr.titech.ac.jp (M. Takahashi).

0022-3115/$ - see front matter © 2006 Elsevier B.V. All rights reserved.
doi:10.1016/j.jnucmat.2006.05.051

an exchange rate of oxygen molecules between the gas and the melt depends on oxygen content in the gas.

A faster response of oxygen concentration with oxygen control may be obtained by immersing solid oxide in the melt in a mass exchanger vessel because of its higher oxygen content [9,10]. The temperature of solid lead oxide (PbO) and the melt is controlled to have desired oxygen solubility. Oxygen concentration becomes equilibrium through dissolution of oxygen into the melt or oxide precipitates from the melt on the solid lead oxide and inner surface of the mass exchanger vessel.

This method allows us not only to control the oxygen concentration but also to measure oxygen solubility in the melt. The experimental data of the oxygen solubility is needed to determine oxygen concentration from measured electromotive force (EMF) of oxygen concentration using a solid-electrolyte type oxygen sensor [11,12]. The oxygen concentration in the melt has been estimated using the correlations of oxygen solubility obtained in Russia [13] and in Germany [14] from measured EMF of the sensor. However, there is no experimental data of the oxygen solubility at low temperature.

The purposes of the present study are to investigate the controllability of oxygen concentration in a flowing Pb–Bi for the mass exchanger type oxygen control system and to determine the oxygen solubility in the liquid Pb–Bi.

2. Experimental

2.1. Pb–Bi forced convection loop

Fig. 1 shows a schematic of a Pb–Bi forced convection test loop used in the present study. The volume of the liquid Pb–Bi in the loop is 22 l. The detail of the loop was described in Ref. [15]. The loop consists of a high temperature region made of STBA26 steel (9Cr–1Mo) and a low temperature region made of SS-316 (18Cr–12Ni–2Mo). The corrosion test section and the oxygen sensor are in the high temperature region, and the expansion tank, the electromagnetic pump and the electromagnetic flow meter [16] are in the low temperature region. A by-pass line that has the electromagnetic flow meter, the bellow valves and the PbO reaction vessel was added in the low temperature region. The temperature of solid PbO particles in the PbO reaction vessel was controlled to have a desired oxygen concentration in the Pb–Bi loop.

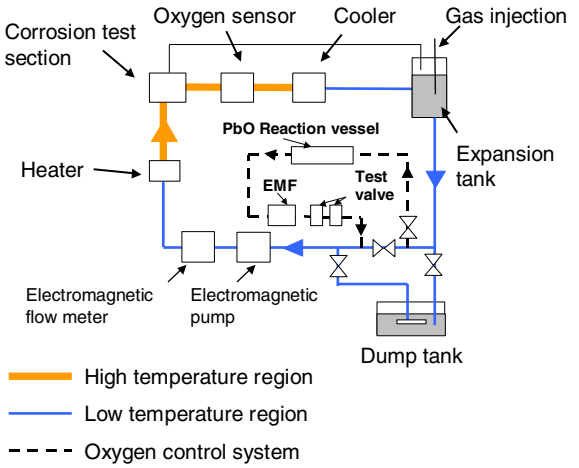

Fig. 1. Pb–Bi corrosion test loop.

Liquid Pb–Bi was circulated by the electromagnetic pump, and the flow rates were measured by the main and by-pass electromagnetic flow meters. The Pb–Bi temperatures at several locations of the loop were monitored using sheathed thermocouples inserted into the flow.

2.2. Oxygen sensor

The oxygen concentration in the melt at the outlet of the corrosion test section was measured by the solid-electrolyte type oxygen sensor. Fig. 2 shows a schematic of the sensor. The sensor cell was made of a solid-electrolyte conductor: yttria stabilized zirconia (Y_2O_3–ZrO_2). In/In_2O_3 and air were tested as reference electrodes in the previous studies [7,8]. In the present experiment, an oxygen-saturated Bi melt

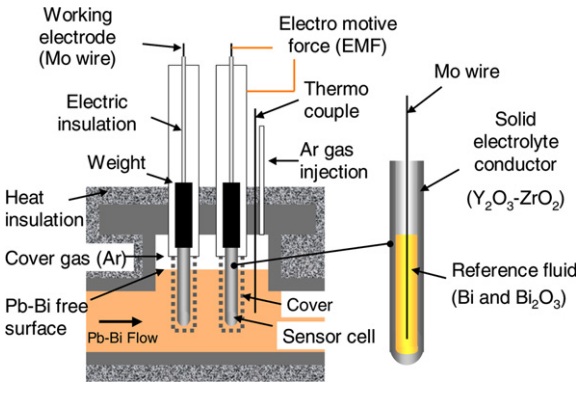

Fig. 2. Oxygen sensor.

($Bi:Bi_2O_3 = 95$ wt%:5 wt%) was used as a reference electrode, and an electrical lead of molybdenum wire was inserted into the Bi melt. The sensor cell was immersed in Pb–Bi for the outer surface of the cell to be exposed to the Pb–Bi flow. EMF or electrical potential between the Mo lead and Pb–Bi (steel vessel wall) was measured using an electrometer with high input impedance of $10^{12}\ \Omega$.

The system of the sensor is expressed by

$$[Bi\text{–}Bi_2O_3]/[Y_2O_3 + ZrO_2]/[Pb\text{–}Bi], \tag{1}$$

where ions of O^{2-} dissolve in Pb–Bi at a certain concentration and in $Bi\text{–}Bi_2O_3$ at saturated concentration. The EMF is induced by the difference of oxygen chemical potential between the inner and outer surfaces of the sensor cell. The EMF is expressed by the Nernst equation:

$$E = \frac{1}{2F}[\Phi_{\mathrm{ref}} - \Phi_{\mathrm{Pb\text{–}Bi}}], \tag{2}$$

where F is the Faraday constant, Φ_{ref} is the potential at the inner surface in the reference fluid, and $\Phi_{\mathrm{Pb\text{–}Bi}}$ is that at the outer surface in Pb–Bi. The chemical reactions in the reference fluid are

$$Bi_2O_3 \leftrightarrow 3O^{2-} + 2Bi^{3+}, \tag{3}$$

and those in the Pb–Bi are

$$O^{2-} + Pb^{2+} \leftrightarrow PbO. \tag{4}$$

If $\Delta G^0_{Bi_2O_3}$ and ΔG^0_{PbO} are the formation energies of Bi_2O_3 and PbO, respectively, the oxygen potentials are given as

$$\Phi_{\mathrm{ref}} = \Delta G^0_{Bi_2O_3}/3, \tag{5}$$

$$\Phi_{\mathrm{Pb\text{–}Bi}} = \Delta G^0_{PbO} + RT_{\mathrm{sensor}} \ln\frac{C}{C_s}, \tag{6}$$

where C is the oxygen concentration in the liquid Pb–Bi, C_s is the saturated concentration or the solubility of oxygen in the Pb–Bi, and T_{sensor} is the temperature of the liquid Pb–Bi at the oxygen sensor in the unit of K. It is probable that Bi oxide is formed in the melt in the present Pb oxide rich condition in the mass exchanger even if the formation energy of Bi oxide is higher than that of Pb oxide. Thus, the following expression of the oxygen potential in Pb–Bi was also taken into account:

$$\Phi_{\mathrm{Pb\text{–}Bi}} = 0.45\Delta G^0_{PbO} + 0.55\frac{\Delta G^0_{Bi_2O_3}}{3} + RT\ln\frac{C}{C_s}. \tag{7}$$

The substitution of Eqs. (5) and (6) into Eq. (2) leads to

$$E = \frac{1}{2F}\left[\frac{\Delta G^0_{Bi_2O_3}}{3} - \Delta G^0_{PbO} - RT_{\mathrm{sensor}}\ln\frac{C}{C_s}\right], \tag{8}$$

and the substitution of Eqs. (5) and (7) into Eq. (2) leads to

$$E = \frac{1}{2F}\left[0.45\frac{\Delta G^0_{Bi_2O_3}}{3} - 0.45\Delta G^0_{PbO} - RT_{\mathrm{sensor}}\ln\frac{C}{C_s}\right]. \tag{9}$$

The oxygen solubility in the liquid Pb–Bi has been provided by Gromov et al. [13] as

$$\log C_s = 1.2 - 3400/T \quad (673\ \mathrm{K} < T < 973\ \mathrm{K}). \tag{10}$$

A theoretical equation was given by Muller et al. [14] as

$$\log C_s = 2.52 - 4803/T. \tag{11}$$

2.3. Oxygen control system

Fig. 3 shows a schematic of the mass exchanger with PbO particles. Three hundred and sixty pieces of spherical PbO particles were mounted in each container between mesh plates in the PbO reaction vessel. The sheathed heater was wound on all of the by-pass line, and the surface temperatures at several positions of the by-pass line were measured with sheathed thermocouples. In the reaction vessel, the sheathed heaters and the thermocouples were inserted for the temperature control and measurement in the melt which contacts with the PbO particles. The outer surface of the reaction vessel was air-cooled to decrease the temperature of the melt in the vessel. The temperature of PbO was nearly equal to that of the melt because of high thermal conductivity of liquid metal. It has been confirmed that temperature difference between the melt in the reaction vessel and the outer surface of the vessel was only about 10 °C, which is low enough as high temperature system. The thermodynamic reactions of the dissolution of oxygen and the precipitation of the oxide occurred on the surfaces of the PbO particles and on the inner wall surface of the vessel.

Table 1 shows the major specifications of the PbO particles. The PbO particles were fabricated in a following procedure: a powder of PbO with a melting point of 888 °C was sintered into lumps at the temperature of 800 °C; and then, the lumps were

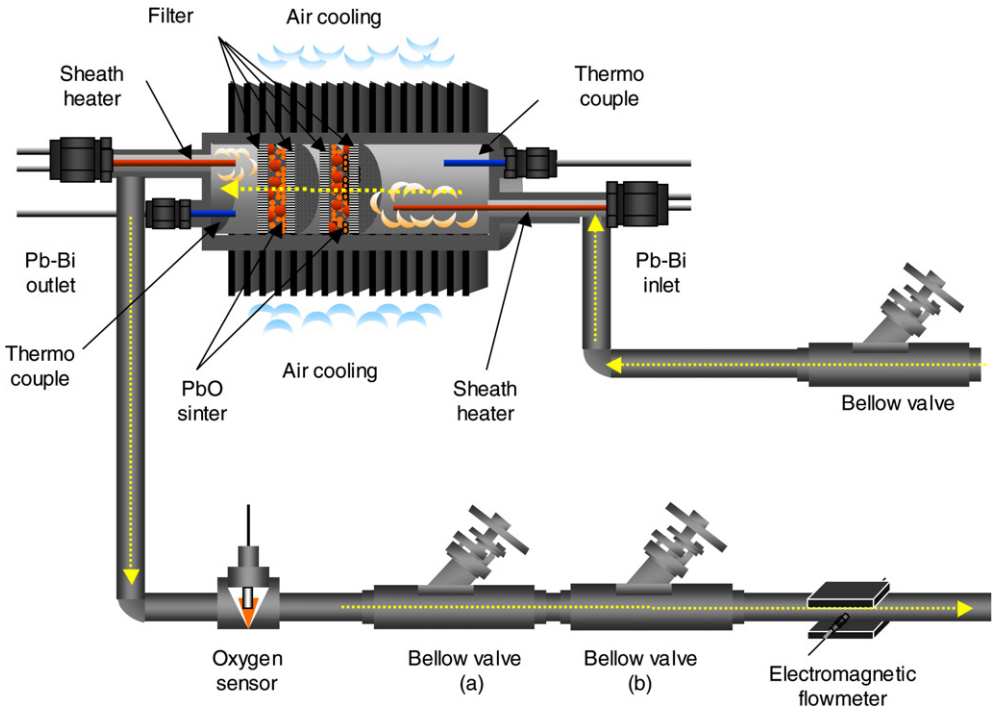

Fig. 3. Schematic of mass exchanger with PbO particles.

Table 1
Specifications of PbO particles

Diameter (m)	$2–4 \times 10^{-3}$
Density (g/m^3)	6.94
Purity (mass%)	99.99
Weight (g)	2.91×10^{-2}
Volume (m^3)	4.19×10^{-9}

mechanically broken into small pieces with rough surfaces. Total surface area of PbO particles in the vessel was estimated as 9.08×10^{-2} m^2.

2.4. Experimental procedure

The oxygen control test was performed at the conditions presented in Table 2. The circulation loop was heated up to 250 °C, and the liquid Pb–Bi was charged from the dump tank into the loop at a flow rate of approximately 0.5 l/min by pressurizing the dump tank at 0.18 MPa with the loop pressure of 0.02 MPa. Then, the Pb–Bi was circulated and heated up to the temperature of the experimental condition. A flowing liquid Pb–Bi in the PbO reaction vessel in the by-pass loop was kept at 250 °C using the air cooler during the heat up operation.

Table 2
Experimental conditions of oxygen control test

Temperature of Pb–Bi in high temperature region (°C)	500
Temperature of Pb–Bi in low temperature region (°C)	400
Temperature of Pb–Bi in PbO reaction vessel (°C)	280–350
Flow rate in circulation loop (l/min)	3
Flow rate in diverged PbO reaction vessel (l/min)	0.5

Measurements were made with the parameter of the temperature in the PbO reaction vessel under constant Pb–Bi temperature at the oxygen sensor.

3. Experimental results

Figs. 4a–4c show the measured EMF of the sensor with time that changed with temperature of the Pb–Bi in the PbO reaction vessel.

In order to evaluate the performance of the mass exchanger type oxygen control system, the response of the EMF of oxygen sensor to the PbO reaction temperature was measured with various temperatures at short intervals as shown in Fig. 4a. The

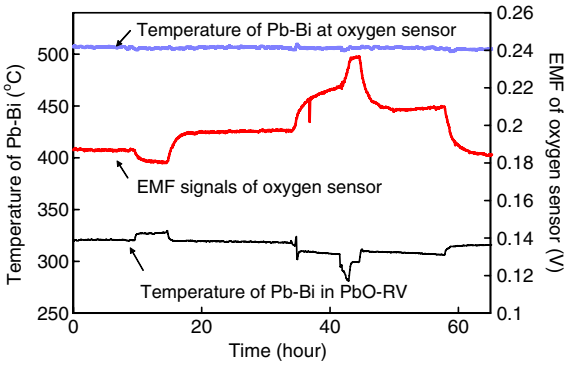

Fig. 4a. EMF transient due the change of reaction temperature between 275 °C and 330 °C.

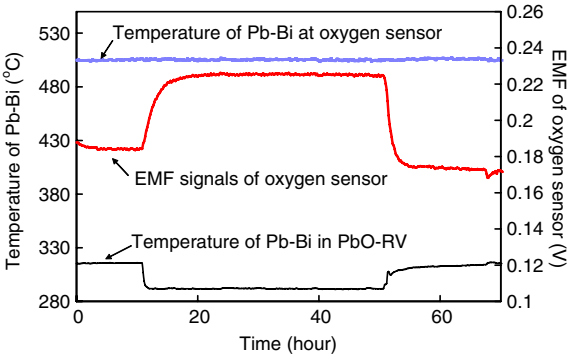

Fig. 4b. Stable EMF transient according to the change of reaction temperature between 275 °C and 320 °C.

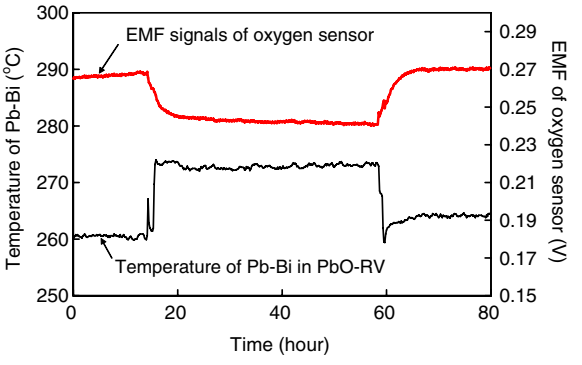

Fig. 4c. EMF signals of oxygen sensor at low temperature of PbO.

EMF output was constant at 0.18 V at the constant reaction temperature of 320 °C. Shortly after the Pb–Bi was heated up to 330 °C in the reaction vessel, the EMF decreased to 0.17 V. And, the EMF reached constant within 3 h. When the temperature was decreased from 330 °C to 320 °C, the EMF increased up to 0.195 V.

Similarly, when the liquid Pb–Bi in the reaction vessel was cooled down from 320 °C to 310 °C at the time of 35 h, the EMF increased to nearly 0.22 V and then reached constant value within 8 h.

In the cooled down process at the time of 45 h, the EMF of approximately 0.21 V lower than that at the time of approximately 40 h was obtained. After the 5 h, the signals reached constant. At the time of 60 h, Pb–Bi in the reaction vessel was heated up to 315 °C. The negative curve was similar to the former one.

The oxygen control test was performed with longer intervals to investigate the stability of the oxygen control system. The result is shown in Fig. 4b. The EMF transited from 0.19 V to 0.23 V following the Pb–Bi temperature shift from 315 °C to 290 °C, and became constant in 5 h. Then, under constant conditions the signal was constant for 40 h, although the EMF fluctuated a little due to slight temperature changes.

In the heat up process from 290 °C to 315 °C, the EMF decreased to the value lower than the previous one at 315 °C, which lead to an increase in oxygen concentration. After 3 h, the EMF reached constant.

Fig. 4c shows the result of the mass exchanger operation at the temperature of about 260 °C with the temperature difference of 240 °C in the loop. At the operation time of 10 h, the Pb–Bi in the reaction vessel was heated from 260 °C up to 275 °C. Then the EMF changed from 0.27 V to 0.24 V. The signals reached constant within 3 h. After the time of 60 h when Pb–Bi in the reaction vessel was cooled down from 275 °C to 265 °C, the EMF increased from 0.24 V to 0.27 V, and the signals reached constant within 10 h.

4. Discussion

4.1. Response of PbO reaction to oxygen sensor

The sensor signal quickly responded to the temperature change of the mass exchanger. The increase in the oxygen concentration in the heat up process was more rapid than that in the cool down process as shown in Figs. 4a–4c. It suggests that the dissolution of oxygen from the PbO to liquid Pb–Bi is more rapid than the oxide precipitation in the melt in the reaction vessel.

However, the response of both of them is fast enough to keep the oxygen concentration in the

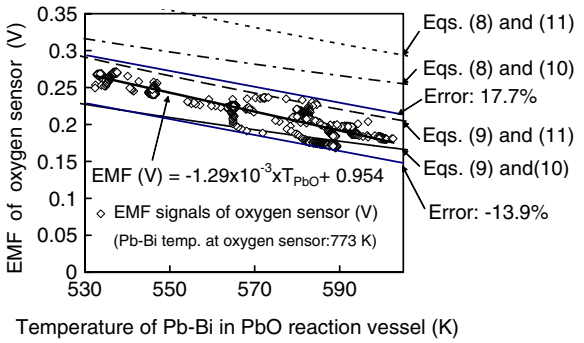

Fig. 5. Comparison of calculated and measured EMF.

adequate region for the formation of the protective oxide layer.

4.2. Oxygen solubility in Pb–Bi

Fig. 5 depicts the dependence of the EMF output at 500 °C on the temperature of the liquid Pb–Bi in the PbO reaction vessel. The EMF decreased linearly with the temperature. By the least square method, the empirical correlation of the EMF, $E_{\text{experiment}}$ is derived as

$$E_{\text{experiment}} = -1.29 \times 10^{-3} T_{\text{PbO}} + 0.954, \tag{12}$$

within the accuracy of 17.7%, where T_{PbO} is the temperature of the Pb–Bi which contacted with the PbO particles in the unit of K. The error is mainly caused by temperature control error in the vessel.

The measured EMF was compared with Eqs. (8)–(11) in Fig. 5. The measured EMF agreed better with Eq. (9) than with Eq. (8). This means that Bi might have a certain effect on the oxidation or the oxide precipitation even if Pb is oxidized at the oxygen potential lower than that of Bi. The Pb–Bi double oxide might be generated in the reaction of oxygen dissolution and precipitation in the melt. This is possibly due to high oxygen potential in the present rich PbO case. Thus, Eq. (12) is equated to Eq. (9) as

$$E_{\text{experiment}} = -1.29 \times 10^{-3} T_{\text{PbO}} + 0.95 = \frac{1}{2F}\left[0.45\frac{\Delta G^0_{\text{Bi}_2\text{O}_3}}{3} - 0.45\Delta G^0_{\text{PbO}} - RT_{\text{sensor}} \ln\frac{C}{C_s}\right]. \tag{13}$$

The oxygen concentration in the melt was measured at 500 °C. Then, the oxygen solubility C_s in the melt at the oxygen sensor in Eq. (13) is expressed using general expression of the oxygen solubility [17] as

$$\log C_s = A + \frac{B}{773}. \tag{14}$$

It can be assumed that the oxygen concentration C in the melt at the sensor is equal to the saturated oxygen concentration in the PbO reaction vessel at the temperature of T_{PbO} that is given by

$$\log C = A + \frac{B}{T_{\text{PbO}}}. \tag{15}$$

The substitution of Eqs.(14) and (15) into Eq. (13) leads to the equation of the EMF as

$$E_{\text{experiment}} = -1.29 \times 10^{-3} T_{\text{PbO}} + 0.95 = 5.77 \times 10^{-2} - 3.33 \times 10^{-2}\left(\ln 10^{\frac{B}{T_{\text{PbO}}} - \frac{B}{773}}\right), \tag{16}$$

where the constant B can be obtained as

$$B(T_{\text{PbO}}) = 10.79 \times 10^{-2} T^2_{\text{PbO}} - 115.43 T_{\text{PbO}} + 26282. \tag{17}$$

as shown in Fig. 6.

The experimental EMF is equal to the theoretical EMF with Eqs. (9) and (10) as

$$E_{(\text{Eqs. (9) and (10)})} = E_{(\text{Eqs. (13), (14) and (17)})}. \tag{18}$$

Then, Eq. (18) is replaced by the third term in the right hand side of Eq. (7) as

$$\ln\frac{C}{C_{s_{(\text{Eq. (10)})}}} = \ln\frac{C}{C_{s_{(\text{Eqs. (14) and (17)})}}}, \tag{19}$$

where the oxygen concentration C in the melt is the same. Then, the constant A is expressed as

$$A_1(T_{\text{PbO}}) = -1.65 \times 10^{-4} T^2_{\text{PbO}} + 1.76 \times 10^{-1} T_{\text{PbO}} + 44.97 \tag{20}$$

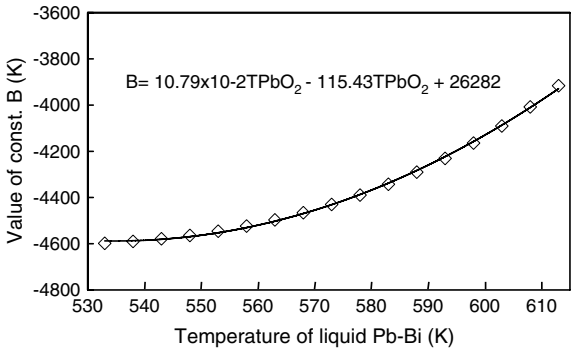

Fig. 6. Derivation of equation for constant B.

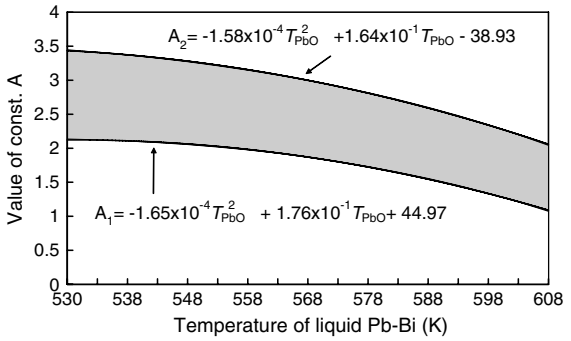

Fig. 7. Derivation of range of constant A.

and shown in Fig. 7. When the other equation for the oxygen solubility of Eq. (11) is used to evaluate the experimental EMF, the constant A can be derived as

$$\ln\frac{C}{C_{s_{(\text{Eq.(11)})}}} = \ln\frac{C}{C_{s_{(\text{Eqs.(14) and (17)})}}}. \tag{21}$$

The constant A different from Eq. (21) can be obtained as

$$A_2(T_{\text{PbO}}) = -1.58\times10^{-4}T_{\text{PbO}}^2 + 1.64\times10^{-1}T_{\text{PbO}} - 38.93. \tag{22}$$

The constant A obtained in the present work is expressed as a band in Fig. 7. This is because the measured EMF data exist between theoretical EMF with Eqs. (10) and (11) in Fig. 5.

The result for the oxygen solubility C_s in the temperature range from 260 °C to 330 °C is shown in Fig. 8 and compared with Eqs. (10) and (11).

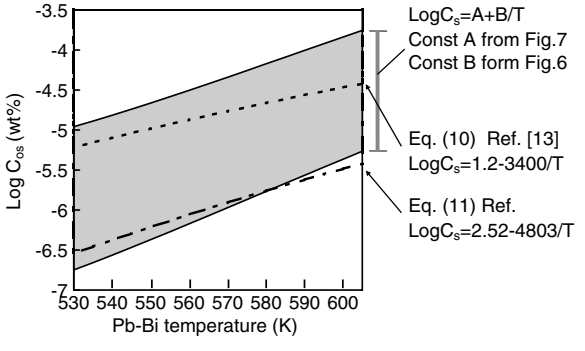

Fig. 8. Comparison between the range of present oxygen solubility equation and previously reported equations [8,9].

5. Conclusion

Major conclusions are as follows:

1. The electromotive force of the oxygen sensor responded to the temperature change of the mass exchanger in short time.
2. The transition of electromotive force in temperature increasing process where oxygen dissolved was completed within the period of 5 h which was shorter than that in temperature decreasing process where oxide precipitated.
3. The electromotive force $E_{\text{experiment}}$ depended on the PbO temperature T_{PbO} linearly. The measured data could be expressed by $E_{\text{experiment}} = -1.29\times10^{-3}T_{\text{PbO}} + 0.95$ with T_{PbO} in K within an accuracy of 17.7%.
4. The measured electromotive force agreed with the calculated results of the Nernst equation using the lead–bismuth double oxide formation energy $\Delta G^0_{\text{Pb–Bi–O equation}}$.
5. The oxygen solubility in liquid lead–bismuth was expressed by $\log C_s = A + B/T$, where the constant A ranged from -4000 to -4600, and the constant B ranged from 1 to 3.5 depending on the reaction temperature.

References

[1] M. Takahashi, T. Obara, T. Iguchi, A. Otsubo, M. Kondo, Y. Qi, K. Hata, K. Hara, S. Uchida, H. Osada, Y. Kasahara, K. Matsuzawa, N. Sawa, Y. Yamada, K. Kurome, Y. Okubo, in: Proc. of Int. Conf. of ICAPP'04, June 13–17, Pittsburgh, PA, 2004, p. 4058.
[2] S. Uchida, H. Osada, Y. Kasahara, M. Takahashi, K. Hata, in: Proc. of 11th Int. Conf. Nuc. Eng. (ICONE11), 20–23 April, Tsukuba, Tokyo, Japan, 2003, p. 36320.
[3] B.F. Gromov, Yu.S. Belomitcev, E.I. Yefimov, M.P. Leonchuk, Yu.I. Orlov, Yu.I. Pankratov, Yu.G. Pashkin, G.I. Toshinski, V.V. Chekunov, B.A. Shmatko, V.S. Stepanov, Nucl. Eng. Design 173 (1997) 207.
[4] K. Kikuchi, T. Sasa, S. Ishikura, K. Mukugi, T. Kai, N. Ouchi, I. Ioka, J. Nucl. Mater. 296 (2001) 34.
[5] Luciano Cinotti, Giuseppe Gherardi, J. Nucl. Mater. 301 (2002) 8.
[6] M. Kondo, M. Takahashi, T. Suzuki, K. Ishikawa, K. Hata, S. Qiu, H. Sekimoto, J. Nucl. Mater. 343 (2005) 349.
[7] M. Kondo, M. Takahashi, N. Sawada, K. Hata, J. Nucl. Sci. Technol. 43 (2005) 107.
[8] M. Takahashi, H. Sekimoto, K. Ishikawa, N. Sawada, T. Suzuki, K. Hata, S. Yoshida, S. Qiu, T. Yano, M. Imai, in: Proc. of 10th Int. Conf. on Nucl. Eng. (ICONE10), 14–18 April, Arlington, Virginia, USA, 2002, p. 22226.
[9] Z.I. Yemelyantseva, V.N. Lenonv, A.D. Yefanov, Y.I. Orlov, P.N. Martynov, V.A. Gulevsky, in: Proc. of 11th

Int. Conf. Nucl. Eng. (ICONE11), 20–23 April, Tokyo, Japan, 2003, p. 36408.
[10] G. Ilincev, J. Nucl. Eng. Sci. 217 (2002) 167.
[11] M. Kondo, M. Takahashi, in: Proc. of Int. Conf. of Global 2005, 9–13 October, Tsukuba, Japan, 2005, p. 503.
[12] J. Konys, H. Muscher, Z. Vob, O. Wedemeyer, J. Nucl. Mater. 296 (2001) 289–294.
[13] B.F. Gromov, Y.I. Orlov, P.N. Martynov, V.A. Gulevski, in: Proc. of HLMC 1999, 1999, p. 87.
[14] G. Muller, A. Heinzel, G. Schumacher, A. Weisenburger, J. Nucl. Mater. 321 (2003) 256.
[15] M. Takahashi, N. Sawada, H. Sekimoto, N. Kotaka, T. Yano, S. Uchida, K. Hata, T. Suzuki, in: Proc. of 8th Int. Conf. on Nucl. Eng. (ICONE8), 2–6 April, Baltimore, MD, 2000, p. 8507.
[16] M. Kondo, M. Takahashi, Prog. Nucl. Eng. 47 (2005) 639.
[17] N. Li, J. Nucl. Mater. 300 (2003) 73.